Manuscript Published in *Journal of Geophysical Research: Oceans*

Investigations of Aerobic Methane Oxidation in Two Marine Seep Environments Part 1: Chemical Kinetics

E. W. Chan[1,6], A. M. Shiller[2], D. J. Joung[2], E. C. Arrington[3], D. L. Valentine[4], M. C. Redmond[5], J. A. Breier[6], S. A. Socolofsky[7], J. D. Kessler[1]

[1]Earth and Environmental Sciences, University of Rochester, Rochester, NY 14627, USA

[2]Division of Marine Science, University of Southern Mississippi, Stennis Space Center, MS 39529, USA

[3]Interdepartmental Graduate Program in Marine Science, University of California – Santa Barbara, Santa Barbara, CA 93106, USA

[4]Dept. of Earth Science and Marine Science Institute, University of California – Santa Barbara, Santa Barbara, CA 93106, USA

[5]Dept. of Biological Sciences, University of North Carolina Charlotte, Charlotte, NC 28223, USA

[6]School of Earth, Environment, and Marine Sciences, University of Texas Rio Grande Valley, Brownsville, TX 78597 USA

[7]Zachry Dept. of Civil Engineering, Texas A&M University, College Station, TX 77843 USA

Key Points:

- Aerobic methane oxidation was investigated and showed that two moles of oxygen are not required to oxidize one mole of methane.
- After a lag time lasting days to weeks, methane was rapidly oxidized in a few days following first-order chemical kinetics.
- These results appear consistent between different oceanic environments, despite regional variabilities.

Abstract

Microbial aerobic oxidation is known to be a significant sink of marine methane (CH_4), contributing to the relatively minor atmospheric release of this greenhouse gas over vast stretches of the ocean. However, the chemical kinetics of aerobic CH_4 oxidation are not well established, making it difficult to predict and assess the extent that CH_4 is oxidized in seawater following seafloor release. Here we investigate the kinetics of aerobic CH_4 oxidation using mesocosm incubations of fresh seawater samples collected from seep fields in Hudson Canyon, US Atlantic Margin and MC118, Gulf of Mexico to gain a fundamental chemical understanding of this CH_4 sink. The goals of this investigation were to determine the response or lag time following CH_4 release until more rapid oxidation begins, the reaction order, and the stoichiometry of reactants utilized (i.e., CH_4, oxygen, nitrate, phosphate, trace metals) during CH_4 oxidation. The results for both Hudson Canyon and MC118 environments show that CH_4 oxidation rates sharply increased within less than one month following the CH_4 inoculation of seawater. However, the exact temporal characteristics of this more rapid CH_4 oxidation varied based on location, possibly dependent on the local circulation and biogeochemical conditions at the point of seawater collection. The data further suggests that methane oxidation behaves as a first-order kinetic process and that the reaction rate constant remains constant once rapid CH_4 oxidation begins.

Plain Language Summary

In and below the seafloor resides the largest global reservoir of methane, a potent greenhouse gas. Following the release of methane from the seafloor, a significant fraction dissolves in the overlying seawater and is oxidized by indigenous microorganisms, helping to prevent its atmospheric release. However, the timing and chemical requirements for this process to occur are not well established, making it difficult to predict and assess the efficiency of methane oxidation following seafloor release. This study systematically measured the chemical changes that are associated with aerobic methane oxidation in seawater using water collected from regions of active seafloor methane release along the U.S. Atlantic margin and the Gulf of Mexico. These results help to refine our understanding of how quickly and how much methane can typically be oxidized in seawater.

1 Introduction

The atmospheric concentration of methane (CH_4) has increased by a factor of 2.5 from preindustrial levels of ~700 ppb to 1850 ppb today, showing the importance of determining the sources and sinks of this greenhouse gas (Dlugokencky et al., 2011). While the oceans account for only ~1 to 3% (4-15 Tg yr^{-1}) of all atmospheric sources of CH_4 today (Dlugokencky et al., 2011), the CH_4 sequestered in and below the seafloor forms the largest CH_4 reservoir on Earth, whose stability is in part controlled by temperature and pressure (Ruppel and Kessler, 2017). The oceanic CH_4 system is

dynamic with formation mechanisms of CH_4 including thermogenic, biogenic, and abiogenic processes (e.g., Karl et al., 2008; Kelley and Früh-Green, 1999; Sherwood Lollar et al., 2002; Oremland and Taylor, 1978). While seafloor emissions are capable of releasing CH_4 from all of these sources to the overlying waters, the depth below the sea surface, the temperature of the surrounding water, and total CH_4 concentration can cause CH_4 to be trapped in sediments as ice-like clathrate hydrates (Ruppel and Kessler, 2017). Nonetheless, globally significant releases of CH_4 carbon from the seafloor have been hypothesized to have occurred during the geologic past, influencing past climate, and possibly occur today (Ruppel and Kessler, 2017). For example, seafloor CH_4 releases are one possible explanation for the global change in carbon cycle dynamics at the Paleocene-Eocene Thermal Maximum (PETM) (Dickens, 2011; Dickens et al., 1995; Higgins and Schrag, 2006; Zeebe et al., 2016). This hypothesis postulates that CH_4 hydrates were destabilized through deep-ocean warming and that the newly released CH_4 was oxidized in sediments and the overlying water column, injecting globally significant amounts of carbon into the active global carbon system (Dickens et al., 1995). In the modern ocean, seafloor CH_4 releases are likely not insignificant (Ruppel and Kessler, 2017), yet the relatively minimal emission of oceanic CH_4 to the atmosphere indicates active CH_4 oxidation in seawater (Reeburgh, 2007; Valentine, 2011).

The single largest seafloor CH_4 release that was directly observed occurred during the 2010 Deepwater Horizon (DWH) well blowout. In addition to oil, large quantities of CH_4 were emitted into the deep waters of the Gulf of Mexico during this incident, and measurements suggest that the released CH_4 was contained in intrusion layers in the deep Gulf waters (800-1100 m) with minimal direct emission to the atmosphere (Camilli et al., 2010; Crespo-Medina et al., 2014; Kessler et al., 2011; Ryerson et al., 2012; Socolofsky et al., 2011; Valentine et al., 2010; Yvon-Lewis et al., 2011). Several studies investigated the microbial oxidation of released CH_4 in the Gulf waters during and following this release (Crespo-Medina et al., 2014; Du and Kessler, 2012; Dubinsky et al., 2013; Kessler et al., 2011; Rogener et al., 2018; Shiller et al., 2017; Valentine et al., 2010), as other work has shown aerobic CH_4 oxidation to be a substantial removal mechanism for CH_4 entering the ocean water column (e.g. Leonte et al., 2017; de Angelis et al., 1993; Mau et al., 2013; Pack et al., 2015; Valentine et al., 2001). Metatranscriptomes showed a clear increase in hydrocarbon monooxygenase gene expression in late May 2010, providing evidence that the oxidation of CH_4 and another low-molecular-weight alkane had already commenced at 30 days after the onset of the spill (Rivers et al., 2013), while Valentine et al. (2010) suggested that the oxidation of ethane and propane was occurring more rapidly than CH_4 in early June. Also, stable isotope probing experiments were carried out with DWH samples, indicating that methanotrophs responded more slowly compared to other organisms responsible for the oxidation of ethane, propane, and some higher molecular weight hydrocarbons (Redmond and Valentine, 2012).

Kessler et al. (2011) and Du and Kessler (2012) used the decrease in dissolved oxygen (DO) in the deepwater CH_4 and hydrocarbon intrusion layers as a tracer of CH_4 oxidation during the DWH incident and determined that the DO loss integrated over the entire

plume area was sufficient to account for complete oxidation of released CH_4. The Kessler et al. (2011) study also assembled a pseudo-first-order model to predict that the greatest amount of CH_4 oxidation (averaged over the entire deep-water plume) occurred ~60-120 days from the start of the spill, and the more comprehensive DO anomaly data set presented in Du and Kessler (2012) supported the timing of the predicted rapid CH_4 oxidation. Crespo-Medina et al. (2014) presented numerous measurements of CH_4 oxidation rates spanning this entire event, from spring through winter of 2010. The first-order oxidation rate constants produced from their CH_4 oxidation rate measurements (Crespo-Medina et al., 2014) generally support the predicted average values for first-order CH_4 oxidation rate constants (Kessler et al., 2011) up to 70 days after the start of the spill (Figure 1). However, many measured CH_4 oxidation rate constants do not agree with the model for times greater than 120 days after the spill when the dissolved CH_4 concentrations decreased significantly below values measured during active emission from the well. The model implicitly assumed that CH_4 oxidation rate constants were proportional to cell density or the activity of the microbial population involved in aerobic CH_4 oxidation, and thus would increase following CH_4 injection and decrease as the new microbial population was remineralized when CH_4 concentrations decreased (Kessler et al., 2011). However, the measurements suggested that the rate constants remain high following rapid CH_4 oxidation and only decrease over longer timescales (Crespo-Medina et al., 2014; Rogener et al., 2018) (Figure 1). Unfortunately, only two CH_4 oxidation rate measurements were reported in the deep intrusion layer (800-1100 m) during the ~60 to 120-day window when Kessler et al. (2011) predicted that the highest average amounts of CH_4 oxidation would occur, and the dates of collection for those two samples are uncertain (Crespo-Medina et al., 2014). Thus, the investigation presented here was initially motivated by the DWH blowout to provide empirical biogeochemical data to thoroughly characterize the temporal changes in microbial oxidation following a CH_4 release. However, these experiments were designed to not only help interpret the fate of CH_4 following the DWH blowout but also to provide more general information on the chemical kinetics of aerobic CH_4 oxidation.

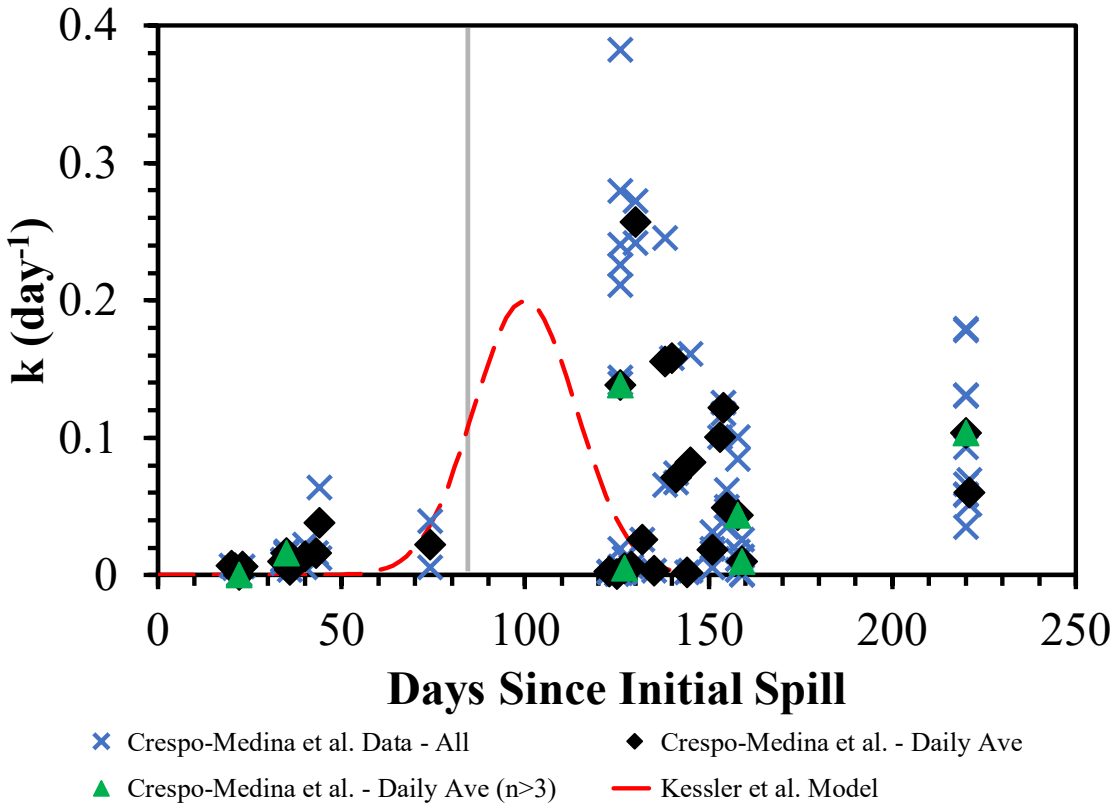

Figure 1. Predicted and measured first-order rate constants for the oxidation of CH_4 released during the Deepwater Horizon blowout (DWH) in the Gulf of Mexico. Here we assume that CH_4 oxidation rate constants vary proportionally to the cell density or activity of the microbial population involved in aerobic CH_4 oxidation. Red dashed line = modeled change in CH_4 oxidation rate constants averaged over the entire deepwater plume from Kessler et al. (2011). Blue × = individual rate constants reported in Crespo-Medina et al. (2014) in the deep plume (800-1100 m water depth). Black Diamond = rate constants, averaged daily, reported in Crespo-Medina et al. (2014) in the deep plume (800-1100 m water depth). Green Triangle = rate constants, averaged daily when the number of data points in a specific day is >3, reported in Crespo-Medina et al. (2014) in the deep plume (800-1100 m water depth). The vertical gray line represents the day the blowout was stopped and no longer emitting CH_4. The lack of empirical data is apparent between 60-120 days after the initiation of the spill when Kessler et al. (2011) predicted the greatest change in methane oxidation rate constants averaged over the entire deepwater plume.

Here we conducted mesocosm experiments with CH_4-laden seawater while measuring the chemical changes over time during CH_4 oxidation events. To assess regional variability in CH_4 oxidation kinetics, seawater was collected in two different locations where CH_4

bubbles were escaping the seafloor: a) Hudson Canyon off the coast of New York and New Jersey near the upper limit of CH_4 hydrate stability and b) the deep Gulf of Mexico near waters once impacted by the DWH blowout (Figure 2). Two goals guided this investigation. The first goal was to determine the chemical kinetics for this oxidation reaction, which included the lag time, or the time between CH_4 exposure and the onset of rapid consumption, and the reaction order. The second goal was to determine the stoichiometry of reactants utilized (i.e., CH_4, oxygen, nitrate, phosphate, trace metals) during CH_4 removal from seawater. The results of these studies can be used to predict the timing of and limitations on CH_4 oxidation following natural or anthropogenic release based on the ambient concentrations of bioactive compounds.

2 Materials and Methods

Waters influenced by known CH_4 seep activity were chosen to examine CH_4 oxidation kinetics. The first research expedition was aboard the R/V *Endeavor* on the North Atlantic Bight from 7-12 July 2014 (Table 1, Figure 2). The recently discovered CH_4 seeps off the coast of New York and New Jersey in Hudson Canyon (HC) (Rona et al., 2015; Skarke et al., 2014; Weinstein et al., 2016) provided an appropriate site for these experiments. Water samples were collected both inside the seep field as well as outside of HC in waters not directly impacted by CH_4 seeps, as determined by the presence or absence of acoustically detected bubbles (Leonte et al., 2017; Weinstein et al., 2016). The second research expedition was from 9-20 April 2015 aboard the E/V *Nautilus* at the Sleeping Dragon seep field site (MC118) in the Gulf of Mexico (Table 1, Figure 2). MC118 is 17 km from the Deepwater Horizon wellhead and provided physical-chemical conditions similar to what may have been experienced during the DWH blowout in 2010. The results obtained from HC and MC118 were analyzed to determine regional similarities and variabilities in CH_4 oxidation kinetics.

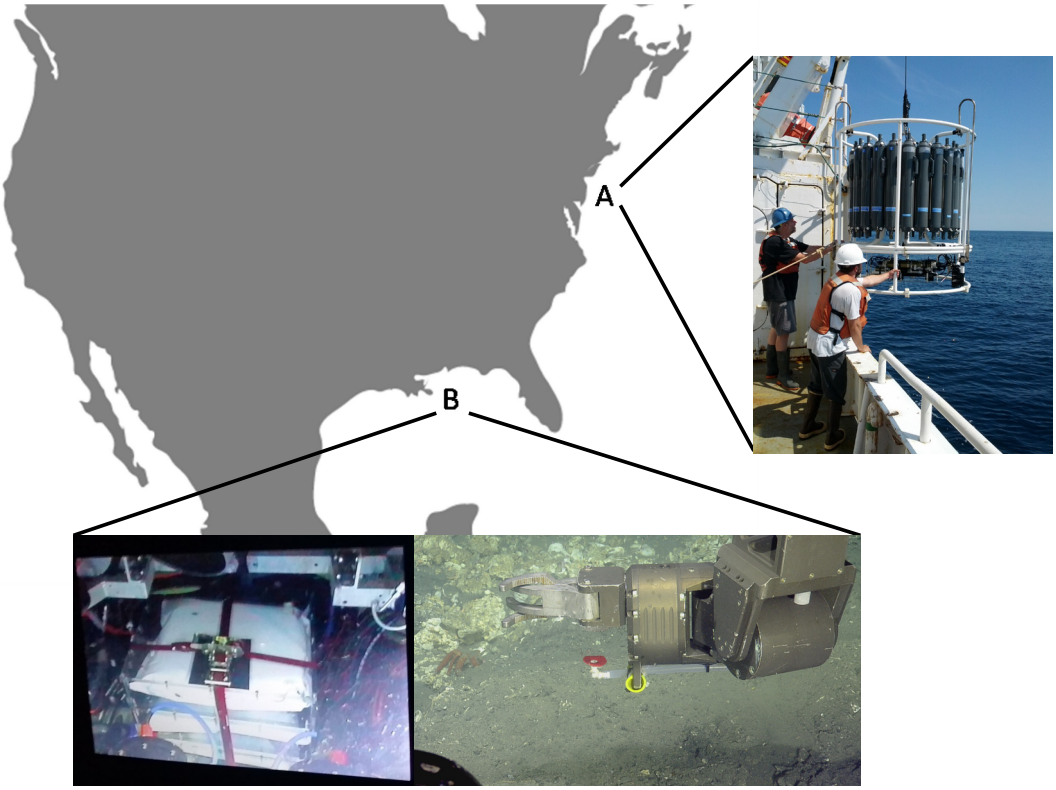

Figure 2. Study locations (A) Hudson Canyon and (B) a gas seep atop Woolsey Mound (a.k.a. Sleeping Dragon) which is part of lease block MC118 in the northern Gulf of Mexico. Seawater samples in Hudson Canyon were collected with Niskin bottles cleaned for trace metal analysis and were used to sample waters that were both directly impacted and not directly impacted by CH_4 seepage. Water from MC118 was collected via ROV in locations visibly impacted by seafloor bubble emissions. On the left are the Mesocosm Incubation System (MIS) cartridges mounted to the chassis of ROV *Hercules*. On the right is the Suspended-Particle Rosette (SUPR) sampler inlet mounted to the starboard manipulator of ROV *Hercules* and methane bubbling upward from the seep site. A bubble-deflecting shield (red disk) was attached to the inlet of the SUPR sampler to collect seawater without collecting gas bubbles.

200 **Table 1.** Hudson Canyon and Sleeping Dragon (MC118) characteristics

Site	Hudson Canyon	Sleeping Dragon (MC118)
Approximate Coordinates	39° 33'N 72° 24'W	28° 51'N 88° 29.5'W
Topography	Semi-enclosed	Open
Sampling Depths (m)	482 – 515	794, 888
Bottom Temperature (°C)	5.25° – 6.24°	5.31° – 8.79°
Sampling Dates	10 July 2014	13-17 April 2015
Sampling Method	Niskin bottles	ROV (SUPR Sampler)
Presence of Oil	No	Yes
Salinity (ppt)	35.01 – 35.05	34.91 – 35.04
In Situ Dissolved Oxygen Concentration Range (μM)	201 – 232	141 – 198
In Situ CH_4 Concentration range (nM)	2.94 – 78.8	51,000 – 221,000
Additional CH_4 Added for Incubation	Yes	No

201

202 **2.1. Incubation and Analysis System**

203 A dissolved gas analyzer system (DGAS) and mesocosm incubation system (MIS) were
204 recently developed (Chan et al., 2016) and were used here to measure the concentration
205 and natural stable isotopes of gases dissolved in seawater throughout mesocosm
206 incubation experiments. (The natural stable isotope results are presented in a companion
207 paper.) In brief, the DGAS unit was developed for the automated analysis of seawater
208 incubations at user-defined intervals, allowing for the relatively high temporal resolution
209 analysis of biochemical changes associated with aerobic CH_4 oxidation. The MIS was
210 developed to house large mesocosm samples in a temperature controlled and clean
211 manner that did not allow gases to diffuse between the sample and the outside
212 environment over the timeframe of this experiment. The MIS contains custom 15 L
213 sample bags that were tested for their cleanliness (i.e., no leaching of trace metals and
214 nutrients) and gas impermeability over time (Chan et al., 2016). They were determined to
215 be a better alternative than borosilicate glass as sample containers for these experiments
216 because the bag material does not leach trace metals, is impermeable to gas exchange,
217 and is of sufficient strength to house sample volumes >10 L. Additionally, since the bags
218 are flexible, aliquots can be periodically removed without contaminating the mesocosm
219 by introducing a headspace for displacement. Since the DWH CH_4 oxidation event
220 occurred over approximately 80 days, mesocosm incubations were designed to contain
221 enough seawater to provide the necessary aliquots for analysis over that same time. To

protect the bags from physical harm and provide a storage solution inside the incubator, the bags were housed in custom-made polycarbonate protective cartridges. In addition, the cartridges provide an easier way to carry the bags during sampling. Once the mesocosms were collected, the DGAS and MIS were connected to analyze the mesocosms based on set intervals thus allowing near real-time dissolved gas concentration and stable isotope measurements (Chan et al., 2016). The dissolved gas concentrations of CH_4, O_2, and CO_2 were measured every few seconds during each mesocosm analysis, and the individual measurements were averaged over a two-minute window. After analysis of the data, it was determined that the DO analyzer manifold malfunctioned during the HC mesocosm incubations, resulting in the DO data from this experiment being sporadically unusable. For this reason, none of the DO data for HC was considered in the biogeochemical analyses. The DO analyzer manifold was redesigned before the MC118 experiments, resulting in usable DO data.

2.2. Mesocosm collection

HC mesocosm experiments were initiated aboard the R/V *Endeavor* from 7 - 12 July 2014. Seawater was collected using trace metal cleaned Niskin bottles with external springs mounted to a CTD rosette (Figure 2; Shiller et al., 2017). Once the samples were back on the ship's deck, two 10 L Niskin bottles were connected to a MIS cartridge to fill with 15 L of seawater. The bags were acid cleaned, rinsed with distilled water, and rinsed with the sample seawater before filling to 15 L with seawater. Water samples were collected from inside the seep field (39° 32.705'N, 72° 24.259'W) and from outside HC in waters not directly influenced by CH_4 seeps (39° 17.236'N 72° 12.080'W). Due to the spatial variance of the seafloor seeps, the initial CH_4 concentrations ranged from 2.94 – 78.8 nM. Therefore, a measured amount (150 ± 1.5 mL) of isotopically standardized CH_4 ($\delta^{13}C$-CH_4 = -20 ‰; Kessler and Reeburgh (2005)) was systemically added to each sample using a mass flow controller and gas filter apparatus to increase dissolved CH_4 concentrations to ca. 300 µM CH_4. These samples were allowed 24 hours to mix and equilibrate inside the MIS before the headspace was removed prior to long-term incubation.

The MC118 mesocosms in the Gulf of Mexico were collected 12 - 17 April 2015 aboard the E/V *Nautilus* located at 28° 51.129'N, 88° 29.51'W directly from seeps at the seafloor between 794 and 888 m depth (Table 1, Figure 2). This experiment was carried out using the Suspended-Particle Rosette (SUPR) sampler (Breier et al., 2009) mounted to the Remotely Operated Vehicle (ROV) *Hercules*. The SUPR sampler is an *in situ* seawater pumping system and was developed to sample dynamic, high gradient, ocean geochemical features at areas such as seep sites. The inlet attached to the ROV arm pumps the seawater into bottles mounted to the SUPR sampler chassis. However, for this study, the system was adapted to pump directly into three of the MIS cartridges mounted to the ROV chassis, which improved the sampling precision substantially (Figure 2). Since samples were taken directly at the seafloor from waters visibly impacted by CH_4 bubbles, the natural dissolved CH_4 concentrations were high (51 to 221 µM); thus it was

not necessary to add additional CH_4 to these mesocosms. This simplified the procedure to incubate the MC118 mesocosms as there was no added headspace equilibration time, in contrast to the HC samples.

2.3. Dissolved Gas Concentration Calculations

The dissolved concentrations of CH_4 measured with the DGAS system give units of ppm (Chan et al., 2016), and it was preferred to convert this into units of μmol of CH_4 L^{-1}. Two independent methods were used to convert the measured ppm concentrations into the molar concentrations of dissolved CH_4. The first method prepared dissolved CH_4 standards by filling mesocosm incubation bags with sterile water containing known concentrations of dissolved CH_4. These CH_4 standards were also stored in the MIS and analyzed with the DGAS system during the mesocosm experiments at sea. Standard calibration curves were determined for each experiment and were used to convert measured ppm units into units of μmol of CH_4 L^{-1}. A second independent technique used the solubility of CH_4 (Wiesenburg and Guinasso, 1979) along with the known volumes of the liquid aliquot and the gaseous headspace being analyzed with the DGAS system to convert the measured ppm concentrations into units of μmol of CH_4 L^{-1}. Both techniques produced similar results. The measured CO_2 concentration values were converted from ppm to μmol of CO_2 L^{-1} following the second technique, but by incorporating the solubility for CO_2 at a salinity of 35 and 5°C (53350 μM atm^{-1}) (Weiss, 1974).

2.4. Microbial community analyses

Samples for DNA analysis were collected by removing 1 L aliquots from the mesocosm experiments at several time intervals and filtering them through 0.22 μm Sterivex filters (Millipore). The filters were stored at -80°C until analysis. DNA was extracted with the FastDNA SPIN Kit for Soil (MP Biomedicals). DNA was quantified with a Qubit 2.0 fluorometer (Life Technologies) and the Qubit dsDNA HS Assay Kit (Thermo Fisher Scientific). Amplification and sequencing of the V4 region of the 16S rRNA gene was done by Seqmatic with the Illumina MiSeq platform (2 x 250 bp), following the protocol described by Caporaso et al. (2011). Sequence analysis was conducted with Mothur version 1.36.0 as described in the MiSeq SOP (Kozich et al., 2013), except that the SILVA (version 123) reference taxonomy was used for classification. This resulted in an average of 149,373 reads per sample. Sequences are available in the Sequence Read Archive under BioProject number PRJNA311933.

Aliquots were taken to detect bacterial cell abundance at various time points throughout both HC and MC118 mesocosms and were enumerated using flow cytometry following the protocol of Wear et al. (2015). Samples were collected in sterile cryovials, preserved with 0.2% final concentration of paraformaldehyde (Electron Microscopy Sciences, Hatfield, Pennsylvania), flash frozen in liquid nitrogen, and stored frozen until analysis. Bacteria were stained with SYBR Green I (Molecular Probes) and enumerated with a BD LSRII flow cytometer (Becton Dickinson, San Jose, California) with an autosampler

attachment. Measurement of bacterial abundances for the HC samples was not successful due to technical failure with the flow cytometer after the preserved samples had already been thawed. However, the MC118 samples were analyzed successfully.

2.5. Macronutrient and Trace Metal Analyses

For each macronutrient analysis, 20 mL of seawater were removed from the mesocosm and passed through a 33 mm diameter syringe filter with a 0.45 μm pore size PVDF membrane (EMD Millipore) and stored frozen in HDPE scintillation vials until analysis. A Lachat Instruments QuikChem 8500 Series 2 Automated Ion Analyzer (Hach) was used by the UCSB Marine Science Institute Analytical Laboratory to obtain nutrient concentrations. Detection limits for nitrate+nitrite (NO_3^-+NO_2^-), ortho-phosphate (PO_4^{-3}), and ammonium (NH_4^+) are 0.20 μM, 0.10 μM, and 0.10 μM, respectively.

Water samples were isolated at interspersed time intervals to quantify the concentration of trace metals in the incubations. The specific trace metals targeted were Mn, Fe, Cu, Zn, Mo, La, Ce, Pr, Nd, Sm, and Eu. For analysis of dissolved trace elements, 7 mL of sample was spiked with a mixture of isotopically-enriched Fe-57, Cu-65, Zn-68, Nd-145, Sm-149, and Eu-153 (Oak Ridge National Labs). Samples were then extracted/pre-concentrated using a SeaFAST system (Elemental Scientific, Inc) operated in offline mode. A similar online SeaFAST extraction procedure is described by Hathorne et al., (2012). The extracted samples were subsequently analyzed using a Thermo-Fisher high-resolution ICP-MS (Element XR) with an Apex-FAST high-efficiency sample introduction system including a Spiro desolvator (Elemental Scientific, Inc.). The enriched isotope spikes allowed for isotope dilution quantification of the spiked elements and also served to provide counts/sec calibration factors for elements that were not spiked with enriched isotopes (Mn, Mo, La, Ce, and Pr). This calibration was also examined with a standard made in dilute nitric acid. Precision and recovery were checked by analysis of a large-volume composite North Atlantic surface seawater sample. Spiked (with a natural isotopic abundance elemental spike) and unspiked aliquots of this sample were analyzed twice in each analytical run. A Ba standard was also run to check for BaO^+ interference on several isotopes and Ba in the extracted samples was also monitored. Due to the extraction resin in the SeaFAST system (Nobias PA-1) discriminating against Ba, in addition to the reduction of the BaO^+ interference by the desolvation system, BaO^+ was less than 0.1% of the counts in Eu-151 and Eu-153. A detailed description of the methods can be found in Shiller et al. (2017) and Ho et al. (2018). Detection limits were typically <1% of the concentrations reported here except for Ce and Eu, where detection limits were <5% of the reported concentrations. Precision (1 σ) was typically ± 2% and recoveries were typically 102 ± 3%.

All data and descriptions of the analyses from these experiments are available through the Gulf of Mexico Research Initiative Information & Data Cooperative (GRIIDC) (Kessler and Chan, 2017).

3. Results

3.1. Chemical Kinetics for Aerobic CH_4 Oxidation

Each incubation was monitored for unambiguous indications of aerobic CH_4 oxidation by assessing changes in dissolved gas concentrations, isotope composition, microbial community composition, cell densities, and micro- and macro-nutrients and this information was used to determine the beginning and ending of more rapid CH_4 oxidation. While all experiments appeared to support microbial growth based on the microbial community composition and changes in cell density, partial blockages in some of the 1/8" tubing used to remove water from the MIS for chemical analysis caused variable results in several specific mesocosms. (To avoid this potential complication, future experiments are advised to insulate the 1/8" tubing when working at temperatures approaching 0°C.) Considered here are the experiments that did not experience such analytical variabilities. Six of the ten mesocosms with waters collected inside and adjacent to HC displayed clear biogeochemical signs of CH_4 oxidation (Figures 3A-B and S1). Four of the ten mesocosms collected with waters at MC118 displayed clear characteristics of CH_4 oxidation (Figures 3C-D and S3-S4).

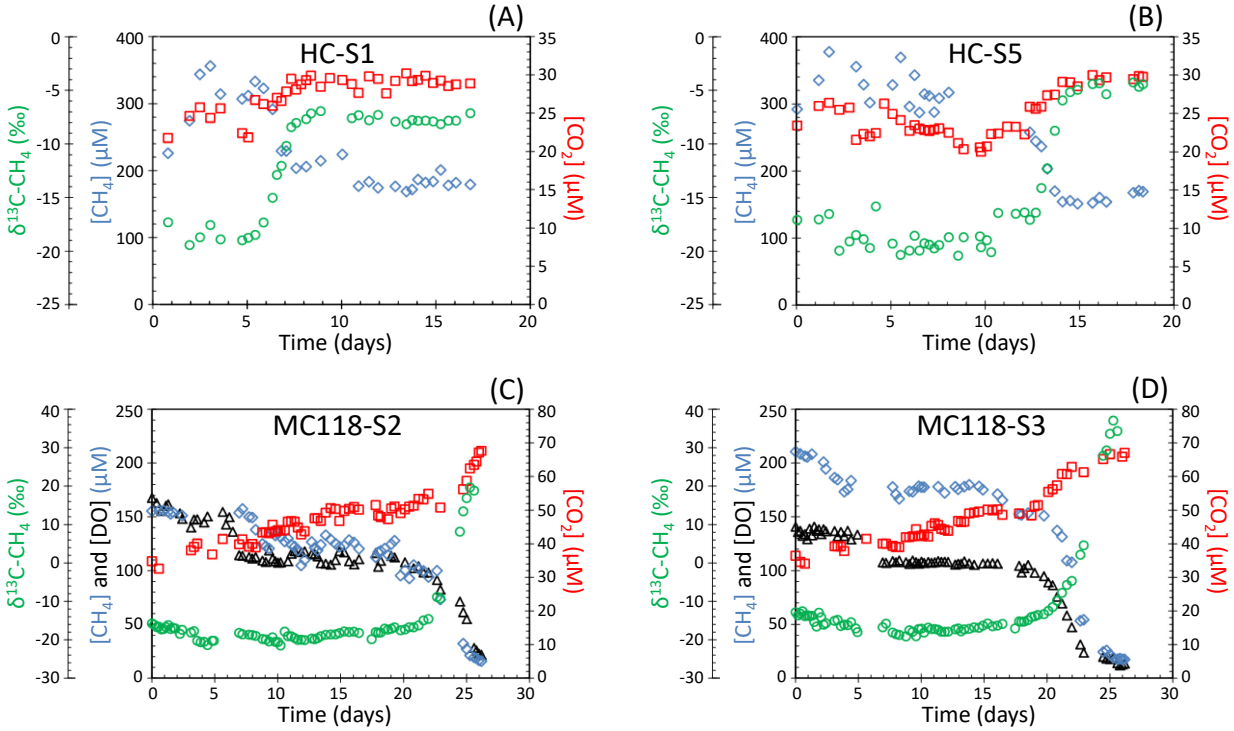

Figure 3. Dissolved concentrations of CH_4 (blue diamonds), CO_2 (red squares), and DO (black triangles), as well as $\delta^{13}C$-CH_4 (green circles) over the course of the incubations. (A) HC-S1 (on seep), (B) HC-S5 (off seep), (C) MC118-S2 (on seep) and (D) MC118-S3

362 (on seep). All data in these figures is available through the Gulf of Mexico Research
363 Initiative Information & Data Cooperative (GRIIDC) (Kessler and Chan, 2017).

364

365

366

367

368

369

370

371

372 **Table 2.** The characteristics for chemical kinetics determined in Hudson Canyon (HC)
373 and MC118. The units for lag time and duration are days, DO:CH_4 is unitless (μM/μM),
374 and first-order oxidation rate constants (k) is day^{-1}.

375

Sample	Location	Lag Time (d)	Duration (d)	DO:CH_4 (molar ratio)	k (day^{-1})
HC-S1	On seep	5.42	2.17	ND	0.25 ± 0.03
HC-S2	On seep	5.43	1.9	ND	0.18 ± 0.04
Ave and Std Dev	On seep	5.43 ± 0.01	2.0 ± 0.2		0.22 ± 0.05
HC-S3	Off seep	14.09	4.05	ND	0.054 ± 0.004
HC-S4	Off seep	12.64	3.05	ND	0.12 ± 0.01
HC-S5	Off seep	12.37	2.53	ND	0.24 ± 0.03
HC-S6	Off seep	8.85	6.34	ND	0.061 ± 0.003
Ave and Std Dev	Off seep	12 ± 2	4 ± 2		0.12 ± 0.09
MC118-S1	On seep	9.60	6.06	0.77	0.107 ± 0.005
MC118-S2	On seep	19.28	5.99	0.81	0.26 ± 0.04
MC118-S3	On seep	18.49	6.78	0.60	0.36 ± 0.04
MC118-S4	On seep	9.82	11.04	0.59	0.20 ± 0.02
Ave and Std Dev	On seep	14 ± 5	7.5 ± 2.4	0.7 ± 0.1	0.2 ± 0.1

376

377 3.1.1. Time to Onset of Rapid CH_4 Oxidation
378 For the Hudson Canyon experiments, seawater was collected from waters impacted by
379 known CH_4 seeps as well as waters outside of Hudson Canyon, not directly impacted by
380 seeps. All samples were incubated at the same near *in situ* temperature (6°C) to determine
381 whether the presence of natural CH_4 seepage influenced methanotrophy. The mesocosms
382 collected at the seep site (samples HC-S1 to -S2) initiated CH_4 oxidation approximately
383 one week faster than the off-seep mesocosms (samples HC-S3 to -S6; Figures 3A-B and
384 S1; Table 2). After the onset of rapid methane oxidation, the on-seep mesocosms
385 depleted their nutrient and trace metal resources and thus completed oxidation in two
386 days on average, whereas the off-seep mesocosms completed oxidation in four days on
387 average (Figure S1 and Table 2). The results from the Atlantic margin suggest that CH_4
388 oxidation can occur in waters with and without the direct influence of CH_4 seeps.
389 However, seeps in a partially enclosed environment such as a submarine canyon, likely
390 keep the waters with a higher starting density of methanotrophic bacteria and thus
391 "primed" for a faster methanotrophic response. This finding appears consistent with
392 previous studies (Leonte et al., 2017; Weinstein et al., 2016).

393 At MC118, since the mesocosms were collected directly from the seep site with an ROV,
394 the waters all contained naturally high concentrations of CH_4 leading us to the hypothesis
395 that CH_4 oxidation would occur more rapidly than in Hudson Canyon. However, this was
396 not the case, with the mesocosms taking 14 days on average to initiate rapid CH_4
397 oxidation and an additional 7.5 days on average until oxidation became limited by a
398 reactant (Figures 3C-D; Figures S3-S4; Table 2). We suspect that the less
399 topographically-restricted MC118 seep field results in more rapid replacement of the
400 ambient waters likely leading to a lower resident methanotrophic population than HC.

401

402 3.1.2. Rate Constants for CH_4 Oxidation

403 For the mesocosms that displayed CH_4 oxidation, we determined whether CH_4 oxidation
404 after the onset of rapid CH_4 oxidation followed zeroth-, first-, or second-order kinetic rate
405 laws as well as the rate constants for the resulting rate law throughout this rapid oxidation
406 process. The procedures used for determining the rate constants can be found in the
407 supporting online information. While the concentration data alone did not clearly
408 distinguish between these reaction orders, the isotope data more clearly indicated that
409 methane consumption followed first-order kinetics (see below and the companion paper).
410 This conclusion is congruent with the Kessler et al. (2011) model and the Crespo-Medina
411 et al. (2014) data from the DWH incident (Figure 1). The HC mesocosms exhibited the
412 highest first-order oxidation rate constant from HC-S1 at 0.25 ± 0.03 day^{-1} and the lowest
413 from HC-S3 at 0.054 ± 0.004 day^{-1}, with an on-seep average of 0.22 ± 0.05 day^{-1} and an
414 off-seep average of 0.12 ± 0.09 day^{-1}. The highest first-order oxidation rate constant at
415 MC118 was MC118-S3 at 0.36 ± 0.04 day^{-1}, the lowest was MC118-S1 at 0.107 ± 0.005
416 day^{-1}, and the average was 0.2 ± 0.1 day^{-1} (Table 2). These rate constants are within the
417 range, but occasionally slightly higher than the rate constants predicted in Kessler et al.

(2011) (0.0001 – 0.200 day^{-1}) and measured in Crespo-Medina et al. (2014) (0.0001 – 0.425 day^{-1}) for CH_4 oxidation in the deepwater plumes during the DWH blowout (Figure 1). Since the rate constants reported here were determined in a closed-system without dilution of cells and substrates, it is not surprising that the rate constants are elevated compared to those determined in the natural environment where such dilution was experienced (Crespo-Medina et al., 2014). It is also interesting to note the differences between the observations here and what was assumed in the Kessler et al. (2011) model. The Kessler et al. (2011) model assumed that the rate constants would increase at the start of rapid CH_4 oxidation and decrease as CH_4 concentrations decreased and this process became reactant limited. However, the empirical data here suggests that the rate constants remain invariant for the remainder of this experiment after the onset of rapid CH_4 oxidation (Table 2, see "Duration" Column for length of time it was invariant), more similar to the rate constant data reported in Crespo-Medina et al. (2014) for the deepwater plumes (Figure 1).

3.1.3. Microbial Community

The goal of the biological analyses was to determine what microbial community was supporting CH_4 oxidation and the extent to which this microbial population bloomed during CH_4 oxidation. To accomplish this goal, changes in bacterial abundance were quantified (Figure 4A) and the 16S rRNA gene was sequenced to determine the composition of the microbial communities (Figure 4B). Comparing these microbial analyses can suggest a growing population of specific microbial communities identified by the 16S rRNA analyses. For both the HC and MC118 mesocosms, the overall results suggest a growing population of organisms previously linked to CH_4 oxidation over the course of these incubations. All incubations began with an extended lag period typical for required adaptation and growth of the bacteria.

Bacterial abundance measurements for the HC mesocosms were not measured because of the aforementioned technical failure. However, the DNA measurements and the change in respiration rate suggest such a bloom occurred. The DNA samples from the beginning of the incubation had low DNA yields and were difficult to amplify. This contrasts with the DNA samples from the end of the incubation, where the sequencing of the 16S rRNA gene was successful consistent with higher cellular abundances (Table S2). Methylococcales, which have been previously linked to aerobic CH_4 oxidation (e.g., Redmond and Valentine, 2012; Redmond et al., 2010), constituted 78 – 97% of 16S rRNA genes sequenced in HC (Figure 4B). The dominance of organisms previously linked to CH_4 oxidation in the HC incubations is likely due to CH_4 being the primary substrate in these mesocosms.

The MC118 bacterial abundance indicates cellular growth across all mesocosms (Figure 4A). Similar to the HC experiments, Methylococcales was also present in MC118 experiments, and when considered alongside cell abundance, indicates a growing population of organisms previously linked to CH_4 oxidation. While Methylococcales

458 constituted a lower percentage of the microbial community in the MC118 mesocosms
459 compared to the HC mesocosms, the MC118 mesocosms were collected directly from a
460 seep that also emits other oil and gaseous hydrocarbons. Thus, this smaller fraction of
461 putative methanotrophs is presumably due to concurrent blooms of other hydrocarbon
462 degrading species (Figure 4) (Reddy et al., 2012; Redmond and Valentine, 2012;
463 Redmond et al., 2010). Redmond and Valentine (2012) observed very similar
464 communities in samples collected in this region of the Gulf of Mexico during the DWH
465 oil spill. Overall, in addition to a growing population of organisms previously linked to
466 CH_4 oxidation, this data also suggests that for both HC and MC118, a significant amount
467 of the methanotrophic biomass remained when the mesocosms were terminated that had
468 not been fully remineralized to CO_2.

469

470

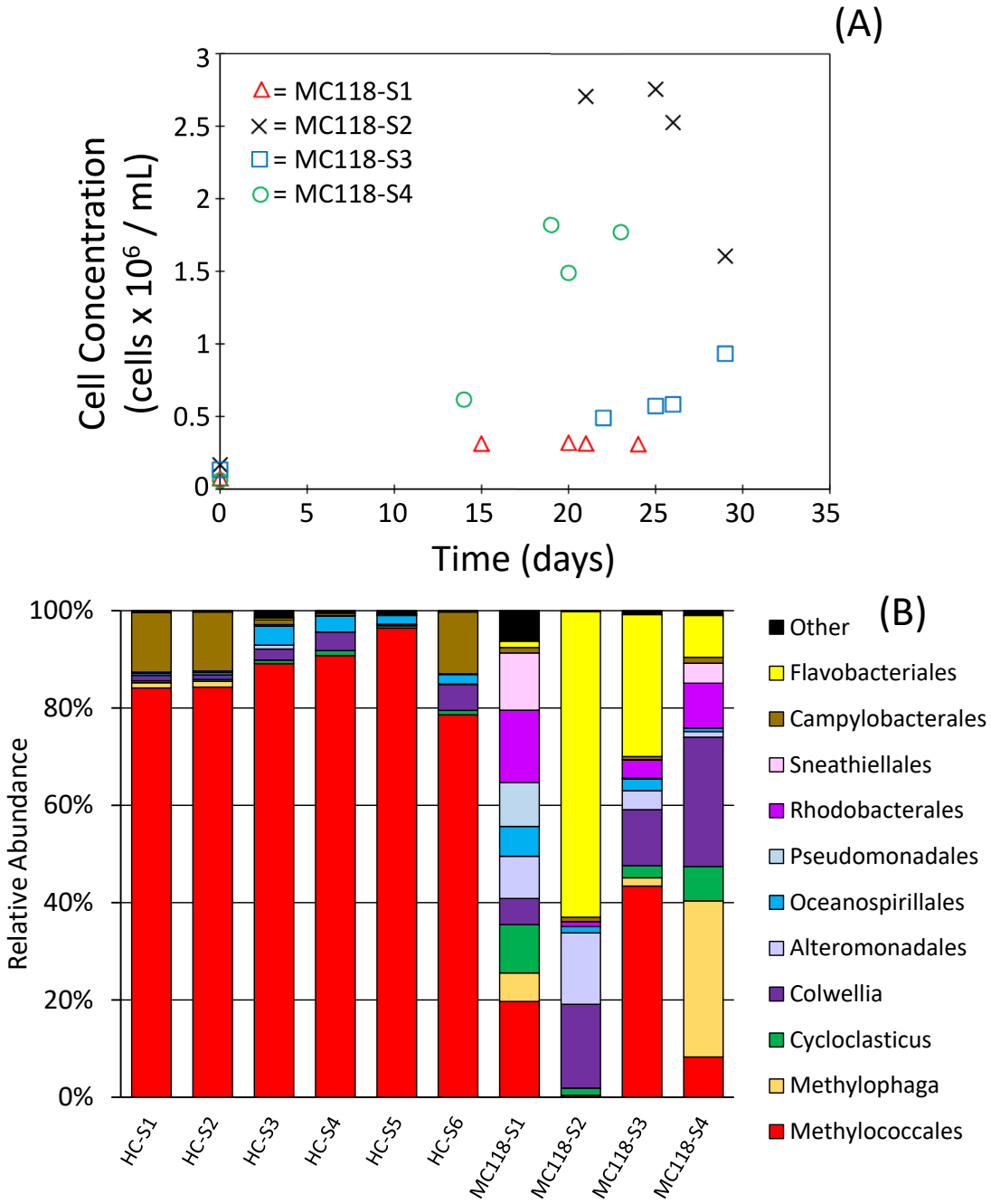

Figure 4. (A) Bacterial abundance across MC118 mesocosm samples. All samples exhibited cellular increases throughout the mesocosm incubations. Red triangles = MC118-S1, black × = MC118-S2, blue squares = MC118-S3, and green circles = MC118-S4. (B) Microbial community compositions (%) from HC and MC118. Data displayed were collected at the end of each mesocosm.

3.2. Amounts of Substrates Required to Oxidize a Quantity of CH_4

3.2.1. General Dissolved Gas Concentration Changes

Of the six mesocosms in HC that exhibited CH_4 oxidation, an average of 98 ± 24 μM (standard deviation of natural variability between mesocosms) of the CH_4 available in each sample was consumed. The average increase in dissolved CO_2 concentration was 4.7 ± 1.4 μM (Table S1).

Since the initial concentration of dissolved CH_4 was variable in the samples collected at MC118 and different from the HC samples, differences in the absolute concentration changes were also observed. Of the four mesocosms that displayed CH_4 oxidation, dissolved CH_4 concentration showed an average decrease of 83 ± 58 μM over the course of the mesocosm experiments. Where there was CH_4 oxidation, there were concomitant decreases in DO and increases in dissolved CO_2 concentrations (Figures 3C-D and S3-S4). On average, the DO decreased by 56 ± 38 μM during the incubations from MC118. The average ratio of DO:CH_4 removed in MC118 was 0.7 ± 0.1 (Table 2). Dissolved CO_2 being produced further supports the occurrence of CH_4 oxidation, with an average increase of 18 ± 4 μM throughout the MC118 experiments (Table S1).

3.2.2. General Nutrient and Trace Metal Concentration Changes

The starting concentrations of nutrients and Fe in the HC mesocosms were lower than for the MC118 mesocosms. The proximity to the sediment interface and intermittent resuspension of sediment by violent bursts of CH_4 (EV Nautilus, 2015) likely caused these higher concentrations found at MC118 (D'souza et al., 2016), which is especially apparent in the Fe concentrations (Figures 5 and S6-S9). For example, the average starting Fe concentration in the HC was 3.2 ± 1.3 nM whereas MC118 displayed average values of 21 ± 10 nM (Figure 5). Throughout the HC mesocosm incubations, both PO_4^{3-} and NO_3^- had high utilization (Figures 5 and S6) and possibly limited CH_4 oxidation. In contrast, the MC118 incubations did not display a decrease in PO_4^{3-} and NO_3^- to the point of limitation (Figures 5 and S7), but it is worth noting that the starting concentrations of CH_4 were less in MC118 than in HC (Table S1).

The trace metal analysis demonstrated pronounced depletions during all mesocosm incubations. The methanol dehydrogenase (MDH) enzyme that catalyzes the second step in CH_4 oxidation is often Ca(II)-dependent (MxaF type) and methane monooxygenase incorporates Cu and Fe (Fox et al. 1988; Murrell et al. 2000; Ross et al., 2019). However, recent discoveries with methano- and methyl-trophic bacteria have suggested that light rare earth elements (LREE), specifically La, Ce, Pr, Nd, and Sm, may play a significant role in the oxidation of methane and methanol (Huang et al., 2018; Picone and Op den Camp, 2019; Pol et al., 2014). Lanthanum (La), one of the lanthanides identified in CH_4 oxidation studies (Pol et al., 2014; Shiller et al. 2017), had an average decrease of 23 ± 2 pM in the HC mesocosms and 15 ± 2 pM in the MC118 mesocosms (Figures 5, S8, and S9). While La displayed the highest percentage removed, other LREEs that were

removed during the microbial bloom were cerium (Ce), praseodymium (Pr), neodymium (Nd), samarium (Sm), and europium (Eu); these additional LREEs exhibited significant decreases, possibly limiting CH_4 oxidation (Kessler and Chan, 2017). Slightly lower depletions in LREEs at MC118 were observed, which we suspect is due to the lower starting concentrations of CH_4 than in the HC mesocosms. Cu and Fe decreases were also notable at 0.8 to 1.3 nM and 0.7 to 1.8 nM, respectively, in HC mesocosms (Figures 5 and S8). MC118 mesocosms showed larger Fe decreases than HC mesocosms at 6.9 to 22.8 nM, perhaps due to the oxidation of non-CH_4 hydrocarbons (Figures 5 and S9).

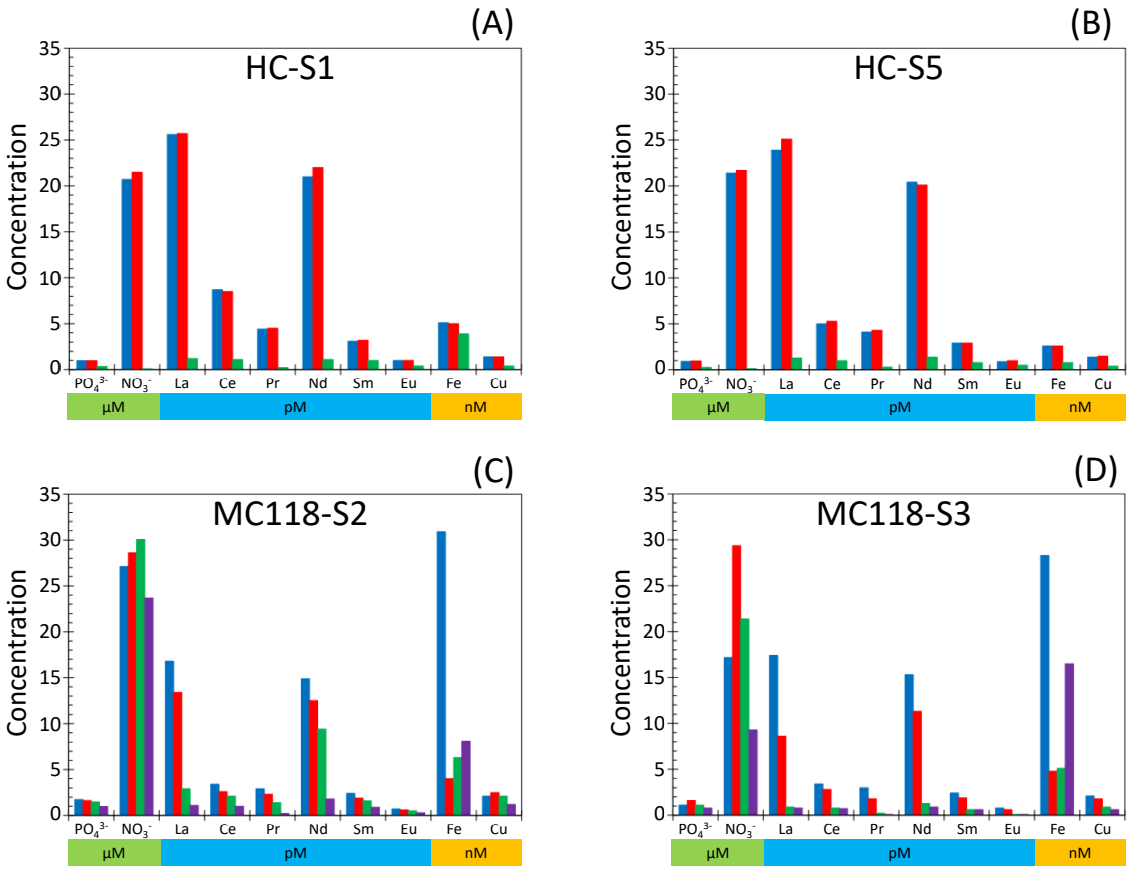

Figure 5. Nutrient and trace metal results from HC and MC118 mesocosms. (A) – (B) Blue = time 0 days sample collected directly from the Niskin bottle, Red = time 0 days sample collected from the mesocosm bag, and Green = samples collected from the mesocosm bag at the end of the incubation, time = 19 – 21 days. The two t = 0 days samples (Blue and Red) were analyzed to determine if there was any nutrient or trace metal contamination associated with the transfer to the sample bags. (C) – (D) Since the MC118 seawater samples were collected directly into the incubation bags, all samples were collected from the bags at different times. Blue = 0 days, Red = 17 – 22 days, Green = 25 days, Violet = 29 days.

4. Discussion

4.1. Mesocosm Stoichiometric Ratios for Aerobic CH_4 Oxidation

An elemental stoichiometric ratio for CH_4 oxidation would be useful for predicting the sufficiency of the environment to supply essential nutrients and trace metals to enable the oxidation of CH_4. For the most accurate determination of a stoichiometric ratio for CH_4 oxidation, the analysis of a pure culture of aerobic methanotrophs would be required. However, using pure culture ratios to predict CH_4 oxidation based on measured concentrations of nutrients or trace metals in the natural environment would be challenging; competing processes in the natural environment, such as denitrification and the oxidation of non-methane hydrocarbons, could also influence changes in these compounds and confuse predictions of the extent of CH_4 oxidation. Furthermore, cultivation tends to favor rapid-growth phenotypes that may lack environmental relevance. Thus, our approach was to use mesocosm incubations so that uncertainties due to these competing processes and potential cultivation bias would be included in the final results. So, while our mesocosm approach likely incurs more uncertainty for a stoichiometric ratio specific to CH_4 oxidation, the intent was that it would provide a reasonable range of possible concentration changes to be observed during an aerobic CH_4 oxidation event in the natural environment. Since concentration changes in DO, CH_4, nutrients, and trace metals were determined throughout these incubations, two different ratios were established, one for CH_4-to-nutrients and another for CH_4-to-trace metals (Table 3).

The CH_4:N:P ratios for HC were similar for both the on- and off-seep sampling locations, with an average ratio of (144 ± 45):(30 ± 5):(1). The CH_4:DO:N:P ratio for MC118 mesocosms was (210 ± 190):(140 ± 110):(19 ± 11):(1). The variability in the MC118 nutrient ratio is likely caused by variable competition for the available nutrients coupled with the oxidation of non-methane hydrocarbons. Due to the relatively elevated uncertainty in the MC118 ratio, the nutrient ratios are statistically similar between HC and MC118. Similar conclusions are reached when investigating the ratio of CH_4:DO:La:Ce:Pr:Nd:Sm:Eu:Fe:Cu, in that the results from HC were statistically similar to MC118, given the variability observed in these environments (Table 3). Increased uncertainty in the MC118 trace metal stoichiometric ratio for CH_4 oxidation was most apparent in Fe, Cu, and Nd, likely caused by different amounts of oxidation of non-CH_4 hydrocarbons. It is interesting to note that Pol et al. (2014) showed that La-Ce-Pr-Nd are all utilized similarly, and that the utilization decreased with higher MW elements. However, while our stoichiometric ratios for La:Nd are in roughly equal proportions, our stoichiometric ratios for La:Sm are significantly less than what might have been expected based the results of Pol et al. (2014) yet are likely related to the decreased utilization of heavier REEs (Picone and Op den Camp, 2019) (Table 3).

Although the biogeochemical conditions are different at the sites investigated, the stoichiometric ratios from both the HC and MC118 mesocosms indicate nutrients and

600 trace metals were utilized in similar proportions (Table 3). Despite the MC118
601 incubations also involving the oxidation of non-CH_4 hydrocarbons (Figure 4), the
602 similarity of results is likely caused by CH_4 being the dominant hydrocarbon available for
603 oxidation at the beginning of each mesocosm. This further suggests that the
604 stoichiometric ratios for aerobic CH_4 oxidation presented here can possibly be used to
605 estimate CH_4 consumption at other oceanographic seep sites, even if concurrent
606 (secondary) biochemical processes are occurring. Certainly, future studies investigating
607 the chemical requirements for CH_4 oxidation should also consider monitoring other
608 biochemical processes occurring concurrently such as the oxidation of higher order
609 hydrocarbons and nitrogen transformations (Ward et al., 2013), both of which likely
610 occurred in these experiments. For example, the trace metal analyses reported here
611 displayed changing Mo concentrations and the nutrient analyses displayed increases in
612 nitrite (Kessler and Chan, 2017), possibly related to nitrogen dynamics in these
613 incubations (Bertine, 1972; Collier, 1985).

614

615

616

617

618 **Table 3.** Mesocosm stoichiometric ratios for aerobic methane oxidation. The averages
619 reported, and their associated standard deviations, are weighted to the uncertainties of the
620 HC and MC118 values.

	CH_4	DO	NO_3^-	PO_4^{3-}
HC	144 ± 45	ND	30 ± 5	1
MC118	210 ± 190	140 ± 110	19 ± 11	1
Average	148 ± 44	140 ± 110	28 ± 5	1

621

	CH_4 ($\times 10^6$)	DO ($\times 10^6$)	La	Ce	Pr	Nd	Sm	Eu	Fe	Cu
HC	4.4 ± 1.3	ND	1	0.22 ± 0.07	0.17 ± 0.01	0.78 ± 0.08	0.07 ± 0.02	0.02 ± 0.01	57 ± 21	44 ± 7
MC118	5.3 ± 3.3	3.6 ± 2.2	1	0.26 ± 0.13	0.16 ± 0.03	0.71 ± 0.28	0.08 ± 0.04	0.03 ± 0.01	850 ± 420	40 ± 40
Average	4.5 ± 1.2	3.6 ± 2.2	1	0.23 ± 0.06	0.17 ± 0.01	0.77 ± 0.08	0.07 ± 0.02	0.03 ± 0.01	60 ± 20	44 ± 7

622

4.2. Evaluating the Reaction Chain for Aerobic CH_4 Oxidation to Interpret the Observed DO:CH_4

The overall reaction for aerobic CH_4 oxidation is generally described with Eq. 1, indicating that if one mole of CH_4 is fully oxidized to CO_2, two moles of DO will be removed.

Eq. 1. $$CH_4 + 2\,O_2 \rightarrow CO_2 + 2\,H_2O$$

However, if CH_4 is not fully converted to CO_2, for example through the formation of biomass or intermediates, less than two moles of O_2 will be utilized. Only after the biomass/intermediates are mineralized to CO_2 will the full two moles of O_2 be removed. For each of the mesocosm experiments conducted in MC118, the DO:CH_4 ratio was less than two (Table 2), suggesting that the formation of biomass and intermediates was significant. Since both the cell count and 16S rRNA gene survey data also indicate that significant methanotrophic biomass formed during these incubations and was still present when these experiments were terminated (Figure 4), it is not surprising that less DO was removed than would have been expected for complete remineralization to CO_2. What is surprising is that the average values for the DO:CH_4 ratios were slightly less than one (Table 2). While we cannot fully discredit that this slight deviation from unity is explained by an unidentified analytical error, we instead investigate the reaction mechanism of aerobic CH_4 oxidation to raise possible biochemical explanations.

Since aerobic CH_4 oxidation is a microbially mediated process, biological growth processes occur concurrently, utilizing a portion of the substrates to produce cellular organic matter. It has been well documented that CH_4 oxidation occurs through soluble and particulate CH_4 monooxygenase enzymes (sMMO and pMMO, respectively), and that most type I methanotrophs closely related to those identified in these mesocosms predominantly use the membrane-bound pMMO (Kalyuzhnaya et al., 2013; Murrell et al., 2010). While sMMO function is well documented, the exact mechanism of pMMO is not completely known with only predicted biochemical pathways (Kalyuzhnaya et al., 2013). The first step of the CH_4 oxidation process with pMMO has CH_4 being converted to methanol (CH_3OH, Eq. 2), requiring electron acceptors and donors (i.e., redox cofactors such as Nicotinamide adenine dinucleotide - NAD, Pyrroloquinoline quinone - PQQ, etc. represented simply in the equations here as A and AH_2). Next, methanol is converted to formaldehyde (CH_2O, Eq. 3) via methanol dehydrogenase (MDH) (Bédard and Knowles, 1989; Kalyuzhnaya et al., 2013). Following this step, there are three possible pathways for formaldehyde to be utilized by the cell: (1) assimilation into biomass via the ribulose monophosphate (RuMP) pathway (Eq. 4) (Dalton and Leak, 1985; Kalyuzhnaya et al., 2013; Quayle and Ferenci, 1978), (2) further oxidation to CO_2 (Eq. 5 and 6) (Bédard and Knowles, 1989; Kalyuzhnaya et al., 2013), or (3) assimilation into the serine pathway. Concerning pathway (2), the formaldehyde is converted to formate by formaldehyde dehydrogenase (FalDH) (Eq. 5) (Bédard and Knowles, 1989). Formate is then converted to CO_2 via formate dehydrogenase (FDH, Eq. 6) (Bédard and Knowles, 1989). Thus, CO_2 can be produced and measured in these mesocosms without first forming cellular biomass via the RuMP pathway. However, part of the formaldehyde is used to create biomass in pathway (1) and thus the amount of carbon remaining as biomass must be considered.

To produce a balanced aerobic CH_4 oxidation reaction series, we hypothesize the following stoichiometry. Since three moles of formaldehyde are required for biomass assimilation via the RuMP pathway (Kalyuzhnaya et al., 2013) and one mole of formaldehyde is required for the oxidation to CO_2 via pathway (2), there needs to be a total of four moles of CH_4 and four moles of O_2 that begin this microbially mediated reaction. To balance the system of equations, the oxidization of the biomass that is created must be considered (Eq. 7). In Eq. 7, biomass is more generally represented as a -CH_2O- chain. Lastly, these reactions would not occur without electron transport within a biological system, and thus an equation for a terminal electron acceptor/donor pair is needed. In an aerobic CH_4 oxidation environment, it is DO that serves as this electron acceptor with many electron transport chains, cytochromes, etc. that facilitate this process (Eq. 8). The simplification of this system of equations results in the overall aerobic CH_4 oxidation equation (Eq. 1).

Eq. 2. $$4\,CH_4 + 4\,O_2 + 4\,AH_2 \xrightarrow{pMMO} 4\,CH_3OH + 4\,H_2O + 4\,A$$

Eq. 3. $$4\,CH_3OH + 4\,A \xrightarrow{MDH} 4\,CH_2O + 4\,AH_2$$

Eq. 4. $$3\,CH_2O + 4\,AH_2 \xrightarrow{RuMP} Biomass$$

Eq. 5. $$CH_2O + H_2O + A \xrightarrow{FalDH} CH_2O_2 + AH_2$$

Eq. 6. $$CH_2O_2 + A \xrightarrow{FDH} CO_2 + AH_2$$

Eq. 7. $$3\ Biomass\ (represented\ as -CH_2O-) + 3\,O_2 \rightarrow 3\,CO_2 + 3\,H_2O$$

Eq. 8. $$2\,AH_2 + O_2 \rightarrow 2\,A + 2\,H_2O$$

Based on these hypothesized reactions, the DO:CH_4 ratio should not drop below 1:1. However, the MC118 incubations ended with an average DO:CH_4 of 0.7 ± 0.1. While synergies with other organisms can remove more CH_4 and provide more electron donors, such as anaerobic oxidation of CH_4 linked to denitrification identified near the sediment-water interface (Raghoebarsing et al., 2006; Waki et al., 2002) or aerobic methane oxidization coupled with nitrate reduction in hypoxic environments (Kits et al. 2015), our mesocosms did not have enough dissolved nitrate to account for the extra DO demand. For example, if we assume that nitrate provides oxygen to further oxidize CH_4, the measured decrease in nitrate during the MC118 mesocosms is only sufficient in one of the four mesocosms to raise the DO:CH_4 to 1:1. A DO:CH_4 of less than 1:1 could also be explained if Eq. 2 did not produce water. In this hypothetical reaction mediated with pMMO, the DO:CH_4 in the initial step of aerobic CH_4 oxidation would only be 0.5:1. We note that this stoichiometry is consistent with the first step of the pMMO-catalyzed reaction cycle, but requires differences in the latter stages than assumed for pMMO in biochemical studies (Culpepper and Rosenzweig, 2012; Sirajuddin and Rosenzweig, 2015). While additional systematic experiments are required to confirm the true reaction mechanism and explain the occurrence of DO:CH_4 ratios <1, our data clearly indicates that two moles of DO is not an inherent requirement for the oxidation of one mole of CH_4. Even though the goal of this study

was not to determine cellular biochemical functions in methanotrophs, the hypothesized reaction mechanism produced from these experiments can serve as a starting point for future experiments.

4.3. Deepwater Horizon Implications

The information learned from the mesocosm incubations can be used to better understand the fate of CH_4 dissolved in the deep hydrocarbon intrusion layers during the DWH blowout in the Gulf of Mexico. First, the biogeochemical conditions at the start of the MC118 incubations were likely more similar to the conditions experienced during the DWH blowout than the samples from HC. The nutrient and trace metal concentrations in the MC118 mesocosm were similar to those experienced during the DWH (Joung and Shiller, 2013; Shiller and Joung, 2012) and there was likely competition between methanotrophs and other hydrocarbon oxidizers for available resources. The MC118 mesocosms showed that ca. 80% of the dissolved CH_4 was oxidized in ca. 19-25 days (Tables 2 and S1, Figures 3, S3, and S4). Certainly, outside of these mesocosm incubation bags mixing in the deep Gulf of Mexico would influence these results since mixing would dilute CH_4 concentrations and methanotrophic cell density but would add fresh DO, nutrients, and trace metals into a parcel of CH_4-laden water. Nonetheless, the results presented here display that a near complete oxidation is possible even without added reactants from mixing. Second, the Kessler et al. (2011) model of DWH CH_4 oxidation (Figure 6) suggests that CH_4 oxidation rate constants averaged over the entire plume peaked ca. 20 days after the CH_4 source to the water column stopped. Perhaps coincidently, the highest rate constant determined from the mesocosm experiments presented here for MC118 occurs ca. 20 days after the parcel of CH_4-laden water was isolated (Figure 6). In addition, the magnitude of the oxidation rate constants determined here is in agreement with the model and previous measurements. Third, applying the stoichiometric ratio derived from the HC samples for CH_4 oxidation to Fe concentrations measured in waters during the DWH blowout (0.3 – 2.2 nmol/kg) (Joung and Shiller, 2013) suggests that 23 to 170 μM of CH_4 could potentially be oxidized. Using the stoichiometric ratio derived from the MC118 mesocosms predicts that 2 to 14 μM CH_4 oxidation could be supported. Estimating CH_4 oxidation using decreases in La during the DWH blowout (Shiller et al., 2017) and applying the stoichiometric ratio from HC seeps, respectively, yields 18 to 53 μM of CH_4 oxidation that could be supported, while using the MC118 stoichiometric ratio suggests that 21 to 64 μM of CH_4 oxidation could be supported. The range of estimates for DWH CH_4 oxidation potential is due to the different concentrations of initial reactants in these experiments as well as resource competition with bacteria conducting other concurrent metabolisms. While CH_4 concentrations were heterogeneous over the extent of the deep intrusion layers during the DWH incident, the capacity for DWH CH_4 to be oxidized, as predicted here with the mesocosm results, is greater than all but a handful of measurements of CH_4 concentration during and after conditions of active release from the well (Crespo-Medina et al., 2014; Joye et al., 2011; Kessler et al., 2011; Reddy et al., 2012; Valentine et al., 2010; Yvon-Lewis et al., 2011).

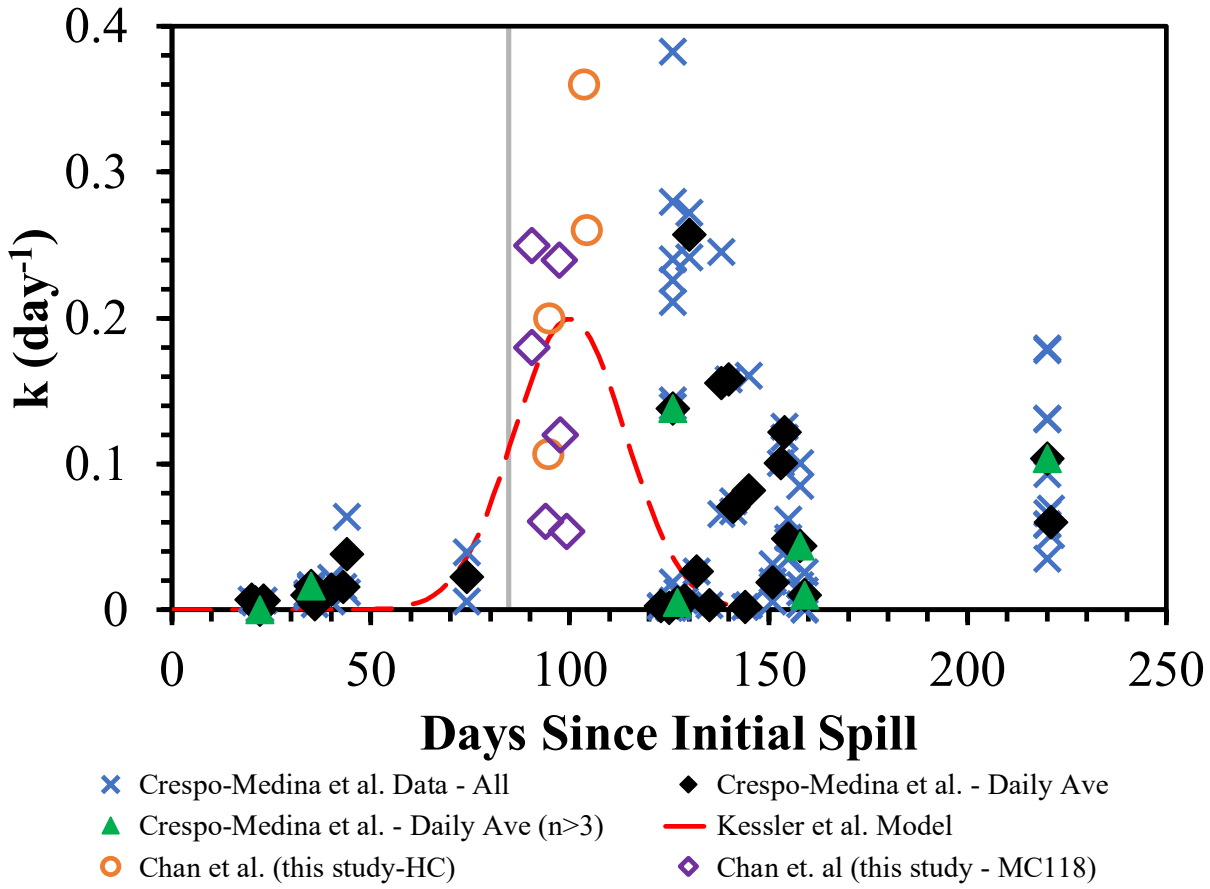

Figure 6. The first-order rate constants for aerobic CH_4 oxidation determined here from HC and MC118 superimposed on the DWH data presented in Figure 1. Violet diamonds = rate constants determined here from the HC experiments. Orange circles = rate constants determined here from the MC118 experiments. All other symbols are the same as indicated in Figure 1. The horizontal (i.e. time in days) position for the data determined here is the time until the start of rapid CH_4 oxidation plotted relative to the day the DWH blowout was stopped and no longer injecting CH_4 into Gulf of Mexico waters (vertical gray line).

Also, if we scale the average concentration of CH_4 removed via oxidation in these mesocosm incubations (90 ± 40 µM) to the entire volume of the deepwater plume during the DWH incident (ca. 7.3×10^{15} L; Du and Kessler, 2012), we can estimate the total capacity for CH_4 oxidation during the DWH incident. This scaling exercise results in a value of $7 \pm 3 \times 10^{11}$ moles of CH_4. Reddy et al. (2012) determined 6.23×10^9 moles of CH_4 were released during the DWH event which is <1% of the CH_4 oxidation potential of the impacted waters. This does not provide proof of the fate of CH_4 during this event; however, it does add further support to our previous contention that DWH CH_4 was fully oxidized in the deep intrusion layers and provides empirical biogeochemical data to characterize an entire oxidation event.

Finally, another result reported here relevant to the DWH blowout is the DO:CH_4 ratio. In MC118 mesocosms, the DO:CH_4 ratios suggest that a significant portion of the oxidized CH_4 is being converted to biomass and potentially intermediates (e.g., methanol) instead of fully to CO_2. Du and Kessler (2012) estimated that 60% ± 40% of the deep intrusion layer hydrocarbon mass

765 was oxidized based on complete conversion to CO_2. However, if a significant portion of this
766 CH_4-C remained as biomass, the DO demand for CH_4 oxidation would have been less, and a
767 near-complete removal of CH_4 could have been supported.
768

769 **5. Conclusions**

770 Mesocosm incubations of seawater collected in two seep fields, one in the North Atlantic Bight
771 in and near Hudson Canyon and the other in the Gulf of Mexico, were used for the controlled
772 study of biogeochemical changes during aerobic CH_4 oxidation. The analysis of dissolved gases
773 (CH_4, CO_2, DO) in real-time and in high resolution permitted monitoring of each mesocosm
774 experiment and provided the opportunity to analyze for other parameters such as microbial
775 genetics, cell abundance, nutrients, and trace metals at critical times during this CH_4 oxidation
776 process. This sampling frequency captured the different stages of these CH_4 oxidation events and
777 was possible due to the controlled and isolated nature of the mesocosm incubations; conducting a
778 similar study of a CH_4 perturbation in nature, such as the DWH blowout, would have been
779 logistically challenging due to more heterogeneous and multi-variate conditions occurring at-
780 depth over an area of approximately 73,000 km^2 (Du and Kessler, 2012).

781 While the initial biogeochemical conditions at the seeps on the Atlantic Margin were different
782 from those in the Gulf of Mexico, several similarities in the characteristics of CH_4 oxidation
783 were observed. The stoichiometric ratio results for CH_4 oxidation were statistically similar
784 between both environments despite greater natural variability in the Gulf of Mexico, likely due
785 to the influence of non-CH_4 hydrocarbon oxidation processes. Both the experiments presented
786 here (Figure 3) and those from the DWH blowout (Figure 1) suggest that a significant lag phase
787 precedes rapid CH_4 oxidation. In the semi-confined environment of Hudson Canyon, this lag
788 time was approximately one week on average while it was approximately two weeks in more
789 open ocean environments outside of Hudson Canyon and in the Gulf of Mexico. Following this
790 lag time, our experiments show that the CH_4 oxidation rate constants increased substantially and
791 remained high even after the CH_4 concentration decreased significantly, a finding which appears
792 congruent with measurements during and after the DWH blowout (Figure 1 and Crespo-Medina
793 et al., 2014; Rogener et al., 2018). Since CH_4 oxidation follows first-order kinetics, the
794 persistence of elevated rate constants suggests that the remineralization of methanotrophic
795 biomass may be slow and thus that CH_4 oxidation could start rapidly without a lag phase, or with
796 an abbreviated lag phase, if CH_4 concentrations again rose, as modeled previously (Valentine et
797 al., 2012). Thus, this data suggests that a natural environment may remain primed to oxidize
798 future releases of CH_4, though the extent and duration remains untested.

799

Acknowledgments

This work was made possible by grants from the National Science Foundation (OCE-1318102 to J.D.K.) and the Gulf of Mexico Research Initiative through the GISR (to J.D.K.) and CONCORDE (to A.M.S.) consortia. Support for D.L.V. and E.C.A. also came primarily from OCE-1318102, but secondary support was provided by the NSF (OCE-1333162 and OCE-1756947). Data are publicly available through the Gulf of Mexico Research Initiative Information & Data Cooperative (GRIIDC) at https://data.gulfresearchinitiative.org/data/R1.x137.000:0019. We thank the captain and crew of the R/V *Endeavor* and the E/V *Nautilus* as well as Bill Fanning and Nicole Raineault for their enthusiasm and support at sea. Finally, we would like to thank Patrick Crill, an anonymous reviewer, and the editor for constructive suggestions which helped to strengthen this manuscript.

References

Bédard, C., & Knowles, R. (1989). Physiology, biochemistry, and specific inhibitors of CH_4, NH_4^+, and CO oxidation by methanotrophs and nitrifiers. *Microbiological Reviews*, *53*(1), 68-84.

Bertine, K. K. (1972). The deposition of molybdenum in anoxic waters. *Marine Chemistry*, *1*(1), 43-53. https://doi.org/10.1016/0304-4203(72)90005-9

Breier, J. A., Rauch, C. G., McCartney, K., Toner, B. M., Fakra, S. C., White, S. N., & German, C. R. (2009). A suspended-particle rosette multi-sampler for discrete biogeochemical sampling in low-particle-density waters. *Deep Sea Research Part I: Oceanographic Research Papers*, *56*(9), 1579-1589. https://doi.org/10.1016/j.dsr.2009.04.005

Camilli, R., Reddy, C. M., Yoerger, D. R., Van Mooy, B. A. S., Jakuba, M. V., Kinsey, J. C., McIntyre, C. P., Sylva, S. P., & Maloney, J. V. (2010). Tracking hydrocarbon plume transport and biodegradation at Deepwater Horizon. *Science*, *330*(6001), 201-204. https://doi.org/10.1126/science.1195223

Caporaso, J. G., Lauber, C. L., Walters, W. A., Berg-Lyons, D., Lozupone, C. A., Turnbaugh, P. J., Fierer, N., & Knight, R. (2011). Global patterns of 16S rRNA diversity at a depth of millions of sequences per sample. *Proceedings of the National Academy of Sciences*, *108*(Supplement 1), 4516-4522. https://doi.org/10.1073/pnas.1000080107

Chan, E. W., Kessler, J. D., Shiller, A. M., Joung, D. J., & Colombo, F. (2016). Aqueous Mesocosm Techniques Enabling the Real-Time Measurement of the Chemical and Isotopic Kinetics of Dissolved Methane and Carbon Dioxide. *Environmental Science & Technology*, *50*(6), 3039-3046. https://doi.org/10.1021/acs.est.5b04304

Collier, R. W. (1985). Molybdenum in the northeast Pacific Ocean. *Limnology and Oceanography*, *30*(6), 1351-1354. https://doi.org/10.4319/lo.1985.30.6.1351

Crespo-Medina, M., Meile, C. D., Hunter, K. S., Diercks, A-R., Asper, V. L., Orphan, V. J., et al. (2014). The rise and fall of methanotrophy following a deepwater oil-well blowout. *Nature Geoscience*, *7*(6), 423-427. https://doi.org/10.1038/NGEO2156

Culpepper, M. A., & Rosenzweig, A. C. (2012). Architecture and active site of particulate methane monooxygenase. *Critical Reviews in Biochemistry and Molecular Biology*, *47*(6), 483-492. https://doi.org/10.3109/10409238.2012.697865

Dalton, H., & Leak, D. J. (1985). Methane oxidation by microorganisms. In R. K. Polle, C. S. Dow (Eds.), *Microbial Gas Metabolism* (pp. 173 – 200). New York: NY: Academic Press.

de Angelis, M. A., Lilley, M. D., Olson, E. J., & Baross, J. A. (1993). *Deep Sea Res. Part I Oceanogr. Res.*, *40*(6), 1169-1186. https://doi.org/10.1016/0967-0637(93)90132-M

Dickens, G. R. (2011). Down the Rabbit Hole: toward appropriate discussion of methane release from gas hydrate systems during the Paleocene-Eocene thermal maximum and other past hyperthermal events. *Climate of the Past*, *7*(3), 831-846. https://doi.org/10.5194/cp-7-831-2011

Dickens, G. R., O'Neil, J. R., Rea, D. K., & Owen, R. M. (1995). Dissociation of oceanic methane hydrate as a cause of the carbon isotope excursion at the end of the Paleocene. *Paleoceanography*, *10*(6), 965-971. https://doi.org/10.1029/95PA02087

Dlugokencky, E. J., E. G. Nisbet, R. Fisher, & D. Lowry (2011). Global atmospheric methane: budget, changes and dangers. *Philosophical Transactions of the Royal Society of London A: Mathematical, Physical and Engineering Sciences*, *369*(1943), 2058-2072. https://doi.org/10.1098/rsta.2010.0341

D'souza, N. A., Subramaniam, A., Juhl, A. R., Hafez, M., Chekalyuk, A., Phan, S., et al. (2016). Elevated surface chlorophyll associated with natural oil seeps in the Gulf of Mexico. *Nature Geoscience*, *9*(3), 215-218. https://doi.org/10.1038/NGEO2631

Du, M., & Kessler, J. D. (2012). Assessment of the spatial and temporal variability of bulk hydrocarbon respiration following the Deepwater Horizon oil spill. *Environmental Science & Technology*, *46*(19), 10499-10507. https://doi.org/10.1021/es301363k

Dubinsky, E. A., Conrad, M. E., Chakraborty, R., Bill, M., Borglin, S. E., Hollibaugh, J. T., et al. (2013). Succession of hydrocarbon-degrading bacteria in the aftermath of the Deepwater Horizon oil spill in the Gulf of Mexico. *Environmental Science & Technology*, *47*(19), 10860-10867. https://doi.org/10.1021/es401676y

EV Nautilus (2015). Explosive Methane Burst and Bubble Streams | Nautilus Live, edited by EVNautilus, *YouTube*. https://youtu.be/pO_rXOEWnAA

Fox, B. G., Surerus, K. K., Münck, E., & Lipscomb, J. D. (1988). Evidence for a mu-oxo-bridged binuclear iron cluster in the hydroxylase component of methane monooxygenase, Mössbauer and EPR studies. *Journal of Biological Chemistry*, *263*(22), 10553-10556.

Hathorne, E.C., Haley, B., Stichel, T., Grasse, P., Zieringer, M., & Frank, M. (2012). Online preconcentration ICP-MS analysis of rare earth elements in seawater. *Geochemistry, Geophysics, Geosystems*, *13*(Q01020). https://doi.org/10.1029/2011GC003907

Huang, J., Yu, Z., & Chistoserdova, L. (2018) Lanthanide-Dependent Methanol Dehydrogenases of XoxF4 and XoxF5 Clades Are Differentially Distributed Among Methylotrophic Bacteria and They Reveal Different Biochemical Properties. *Frontiers in Microbiology*, *9*(1366). https://doi.org/10.3389/fmicb.2018.01366

Higgins, J. A., & Schrag, D. P. (2006). Beyond methane: towards a theory for the Paleocene–Eocene thermal maximum. *Earth Planetary Science Letters*, *245*(3-4), 523-537. https://doi.org/10.1016/j.epsl.2006.03.009

Ho, P., Lee, J., Heller, M., Lam, P.. and Shiller, A. M. (2018). The distribution of dissolved and particulate Mo and V along the U.S. GEOTRACES East Pacific Zonal Transect (GP16): the

roles of oxides and biogenic particles in their distributions in the oxygen deficient zone and the hydrothermal plume. *Marine Chemistry*, *201*, 242-255. https://doi.org/10.1016/j.marchem.2017.12.003

Joung, D., & Shiller, A. M. (2013). Trace element distributions in the water column near the Deepwater Horizon well blowout. *Environmental Science & Technology*, *47*(5), 2161-2168. https://doi.org/10.1021/es303167p

Joye, S. B., MacDonald, I. R., Leifer, I., & Asper, V. (2011). Magnitude and oxidation potential of hydrocarbon gases released from the BP oil well blowout. *Nature Geoscience*, *4*(3), 160-164. https://doi.org/10.1038/NGEO1067

Kalyuzhnaya, M. G., Yang, S., Rozova, O., Smalley, N., Clubb, J., Lamb, A., et al. (2013). Highly efficient methane biocatalysis revealed in a methanotrophic bacterium. *Nature Communications*, *4*, 2785. https://doi.org/10.1038/ncomms3785

Karl, D. M., Beversdorf, L., Björkman, K. M., Church, M. J., Martinez, A., & Delong, E. F. (2008). Aerobic production of methane in the sea. *Nature Geoscience*, *1*(7), 473-478. https://doi.org/10.1038/ngeo234

Kelley, D. S., & Früh-Green, G. L. (1999). Abiogenic methane in deep-seated mid-ocean ridge environments: Insights from stable isotope analyses. *Journal of Geophysical Research – Solid Earth*, *104*(B5), 10439-10460, https://doi.org/10.1029/1999jb900058

Kessler, J. D., & Chan, E. (2017). Chemical and Isotopic Kinetics of Dissolved Methane and Carbon Dioxide for samples collected in the northern Gulf of Mexico and Atlantic July 2014-April 2015. Distributed by Gulf of Mexico Research Initiative Information and Data Cooperative (GRIIDC), Harte Res. Inst., Texas A&M Univ., Corpus Christi, Corpus Christi, https://doi.org/10.7266/N7RR1WPX

Kessler, J. D., & Reeburgh, W. S. (2005). Preparation of natural methane samples for stable isotope and radiocarbon analysis. *Limnology and Oceanography: Methods*, *3*, 408-418. https://doi.org/10.4319/lom.2005.3.408

Kessler, J. D., Valentine, D. L., Redmond, M. C., Du, M., Chan, E.W., Mendes, S.D., et al. (2011). A Persistent Oxygen Anomaly Reveals the Fate of Spilled Methane in the Deep Gulf of Mexico. *Science*, *331*(6015), 312-315. https://doi.org/10.1126/science.1199697

Kits, K. D., Klotz, M. G., & Stein, L. Y. (2015). Methane oxidation coupled to nitrate reduction under hypoxia by the G ammaproteobacterium M ethylomonas denitrificans, sp. nov. type strain FJG1. *Environmental microbiology, 17*(9), 3219-3232. https://doi.org/10.1111/1462-2920.12772

Kozich, J. J., Westcott, S. L., Baxter, N. T., Highlander, S. K., & Schloss, P. D. (2013). Development of a dual-index sequencing strategy and curation pipeline for analyzing amplicon sequence data on the MiSeq Illumina sequencing platform. *Applied and Environmental Microbiology*, *79*(17), 5112-5120. https://doi.org/10.1128/AEM.01043-13

Leonte, M., Kessler, J. D., Kellermann, M. Y., Arrington, E. C., Valentine, D. L., & Sylva, S. P. (2017). Rapid rates of aerobic methane oxidation at the feather edge of gas hydrate stability in the waters of Hudson Canyon, US Atlantic Margin. *Geochimica et. Cosmochimica Acta*, *204*, 375-387. https://doi.org/10.1016/j.gca.2017.01.009

Mau, S., Blees, J., Helmke, E., Niemann, H., & Damm, E. (2013). Vertical distribution of methane oxidation and methanotrophic response to elevated methane concentrations in stratified waters of the Arctic fjord Storfjorden (Svalbard, Norway). *Biogeosciences*, *10*(10), 6267-6278. https://doi.org/10.5194/bg-10-6267-2013

Murrell, J. C., McDonald, I. R., & Gilbert, B. (2000). Regulation of expression of methane monooxygenases by copper ions. *Trends in Microbiology*, *8*(5), 221-225. https://doi.org/10.1016/S0966-842X(00)01739-X

Murrell, J. C. (2010). The aerobic methane oxidizing bacteria (methanotrophs), In K. N. Timmis, T. J. McGenity, J. Roelof van der Meer, & V. de Lorenzo (Eds.), *Handbook of hydrocarbon and lipid microbiology* (pp. 1953-1966), Springer Berlin Heidelberg.

Oremland, R. S., & Taylor, B. F. (1978). Sulfate reduction and methanogenesis in marine sediments. *Geochimica et. Cosmochimica Acta*, *42*(2), 209-214, https://doi.org/10.1016/0016-7037(78)90133-3.

Pack, M. A., Heintz, M. B., Reeburgh, W. S., Trumbore, S. E., Valentine, D. L., Xu, X., & Druffel, E. R. M. (2015). Methane oxidation in the eastern tropical North Pacific Ocean water column. *Journal of Geophysical Research-Biogeosciences.*, *120*(6), 1078–1092. https://doi.org/10.1002/2014JG002900

Picone, N. & Op den Camp, H. J. M. (2019). Role of rare earth elements in methanol oxidation. *Current Opinion in Chemical Biology*, 49, 39-44. https://doi.org/10.1016/j.cbpa.2018.09.019

Pol, A., Barends, T. R. M., Dietl, A., Khadem, A. F., Eygensteyn, J., Jetten, M. S. M., & Op den Camp, H. J. M. (2014). Rare earth metals are essential for methanotrophic life in volcanic mudpots. *Environmental Microbiology*, *16*(1), 255-264. https://doi.org/10.1111/1462-2920.12249

Quayle, J. R., & Ferenci, T. (1978). Evolutionary aspects of autotrophy. *Microbiological Reviews*, *42*(2), 251-273.

Raghoebarsing, A. A., Pol, A., nan de Pas-Schoonen, K. T., Smolders, A. J. P., Ettwig, K. F., Rijpstra, W. I. C., et al. (2006). A microbial consortium couples anaerobic methane oxidation to denitrification. *Nature*, *440*(7086), 918-921. https://doi.org/10.1038/nature04617

Reddy, C. M., Arey, J. S., Seewald, J. S., Sylva, S. P., Lemkau, K. L., Nelson, R. K., et al. (2012). Composition and fate of gas and oil released to the water column during the Deepwater Horizon oil spill. *Proceedings of the National Academy of Sciences*, *109*(50), 20229-20234. https://doi.org/10.1073/pnas.1101242108

Redmond, M. C., & Valentine, D. L. (2012). Natural gas and temperature structured a microbial community response to the Deepwater Horizon oil spill. *Proceedings of the National Academy of Sciences, 109*(50), 20292-20297. https://doi.org/10.1073/pnas.1108756108

Redmond, M. C., Valentine, D. L., & Sessions, A. L. (2010). Identification of novel methane-, ethane-, and propane-oxidizing bacteria at marine hydrocarbon seeps by stable isotope probing. *Applied and Environmental Microbiology, 76*(19), 6412-6422. https://doi.org/10.1128/AEM.00271-10

Reeburgh, W. S. (2007). Oceanic methane biogeochemistry. *Chemical reviews, 107*(2), 486-513. https://doi.org/10.1021/cr050362v

Rivers, A. R., Sharma, S., Tringe, S. G., Martin, J., Joye, S. B., & Moran, M. A. (2013). Transcriptional response of bathypelagic marine bacterioplankton to the Deepwater Horizon oil spill. *ISME Journal*, *7*(12), 2315-2329. https://doi.org/10.1038/ismej.2013.129

Rogener, M. K., Bracco, A. Hunter, K. S., Saxton, M. A., & Joye, S. B. (2018). Long-term impact of the Deepwater Horizon oil well blowout on methane oxidation dynamics in the northern Gulf of Mexico. *Elementa-Science of the Anthropocene*, 6(73). https://doi.org/10.1525/elementa.332

Rona, P., Guida, V., Scranton, M., Gong, D. L., Macelloni, L., Pierdomenico, M., et al. (2015). Hudson submarine canyon head offshore New York and New Jersey: A physical and geochemical investigation. *Deep-Sea Research Part II-Topical Studies in Oceanography*, *121*(SI), 213–232. https://doi.org/10.1016/j.dsr2.2015.07.019

Ross, M. O., MacMillan, F., Wang, J., Nisthal, A., Lawton, T. J., Olafson, B. D., Mayo, S. L., Rosenzweig, A. C., & Hoffman, B. M. (2019). Particulate methane monooxygenase contains only monocopper centers. *Science*, 364(6440), 566-570. https://doi.org/ 10.1126/science.aav2572

Ruppel, C. D. & Kessler, J. D. (2017). The Interaction of Climate Change and Methane Hydrates. *Reviews of Geophysics*, *55*(1), 126-168. https://doi.org/10.1002/2016RG000534

Ryerson, T. B., R. Camilli, J. D. Kessler, E. B. Kujawinski, C. M. Reddy, D. L. Valentine, E. Atlas, D. R. Blake, J. de Gouw, & S. Meinardi (2012). Chemical data quantify Deepwater Horizon hydrocarbon flow rate and environmental distribution. *Proceedings of the National Academy of Sciences*, *109*(50), 20246-20253. https://doi.org/10.1073/pnas.1110564109

Sherwood Lollar, B., T. Westgate, J. Ward, G. Slater, & G. Lacrampe-Couloume (2002). Abiogenic formation of alkanes in the Earth's crust as a minor source for global hydrocarbon reservoirs. *Nature*, *416*(6880), 522-524. https://doi.org/10.1038/416522a

Shiller, A. M., Chan, E. W., Joung, D. J., Redmond, M. C., & Kessler, J. D. (2017). Light rare earth element depletion during Deepwater Horizon blowout methanotrophy. *Scientific Reports*, *7*(1), 10389. https://doi.org/10.1038/s41598-017-11060-z

Shiller, A. M., & Joung, D. J. (2012). Nutrient depletion as a proxy for microbial growth in Deepwater Horizon subsurface oil/gas plumes. *Environmental Research Letters*, *7*(4), 045301. https://doi.org/10.1088/1748-9326/7/4/045301

Sirajuddin, S., & Rosenzweig, A. C. (2015). Enzymatic Oxidation of Methane. *Biochemistry*, *54*(14), 2283-2294. https://doi.org/10.1021/acs.biochem.5b00198

Skarke, A., Ruppel, C., Kodis, M., Brothers, D., & Lobecker, E. (2014). Widespread methane leakage from the sea floor on the northern US Atlantic margin. *Nature Geoscience*, *7*(9), 657-661. https://doi.org/10.1038/NGEO2232

Socolofsky, S. A., Adams, E. E., & Sherwood, C. R. (2011). Formation dynamics of subsurface hydrocarbon intrusions following the Deepwater Horizon blowout. *Geophysical Research Letters*, *38*, L09602. https://doi.org/10.1029/2011GL047174

Valentine, D. L., Blanton, D. C., Reeburgh, W. S., & Kastner, M. (2001). Water column methane oxidation adjacent to an area of active hydrate dissociation. Eel River Basin, *Geochimica et. Cosmochimica Acta*, *65*(16), 2633-2640. https://doi.org/10.1016/S0016-7037(01)00625-1

Valentine, D. L., Kessler, J. D., Redmond, M. C., Mendes, S. D., Heintz, M. B., Farwell, C., et al. (2010). Propane Respiration Jump-Starts Microbial Response to a Deep Oil Spill. *Science*, *330*(6001), 208-211. https://doi.org/10.1126/science.1196830

Valentine, D. L. (2011). Emerging topics in marine methane biogeochemistry. *Annual Review of Marine Science, 3*, 147-171. https://doi.org/10.1146/annurev-marine-120709-142734

Valentine, D. L., Mezić, I., Maćešić, S., Črnjarić-Žic, N., Ivić, S., Hogan, P. J., et al. (2012). Dynamic autoinoculation and the microbial ecology of a deep water hydrocarbon irruption. *Proceedings of the National Academy of Sciences*, *109*(50), 20286-20291. https://doi.org/10.1073/pnas.1108820109

Waki, M., Tanaka, Y., Osada, T., & Suzuki, K. (2002). Effects of nitrite and ammonium on methane-dependent denitrification. *Applied Microbiology and Biotechnology*, *59*(2-3), 338-343. https://doi.org/10.1007/s00253-002-1003-y

Wear, E. K., Carlson, C. A., Windecker, L. A., & Brzezinski, M. A. (2015). Roles of diatom nutrient stress and species identity in determining the short- and long-term bioavailability of diatom exudates to bacterioplankton. *Marine Chemistry*, *177*(2), 335-348. https://doi.org/10.1016/j.marchem.2015.09.001

Weinstein, A., Navarrete, L., Ruppel, C., Weber, T. C., Leonte, M., Kellermann, M. Y., et al. (2016). Determining the flux of methane into Hudson Canyon at the edge of methane clathrate hydrate stability, *Geochemistry, Geophysics, Geosystems, 17*(10), 3882-3892. https://doi.org/10.1002/2016GC006421

Weiss, R. F. (1974). Carbon dioxide in water and seawater: the solubility of a non-ideal gas. *Marine Chemistry*, *2*(3), 203–215. https://doi.org/10.1016/0304-4203(74)90015-2.

1026 Wiesenburg, D. A., & Guinasso Jr., N. L. (1979). Equilibrium solubilities of methane, carbon
1027 monoxide, and hydrogen in water and sea water. *Journal of Chemical and Engineering Data*,
1028 *24*(4), 356-360. https://doi.org/10.1021/je60083a006

1029 Yvon-Lewis, S. A., Hu, L., & Kessler, J. (2011). Methane flux to the atmosphere from the
1030 Deepwater Horizon oil disaster. *Geophysical Research Letters*, *38*, L01602.
1031 https://doi.org/10.1029/2010gl045928.

1032 Zeebe, R. E., Ridgwell, A., & Zachos, J. C. (2016). Anthropogenic carbon release rate
1033 unprecedented during the past 66 million years. *Nature Geoscience*, 9(4), 325-329.
1034 https://doi.org/10.1038/NGEO2681

1035